



## Backbone dynamics of free barnase and its complex with barstar determined by $^{15}\text{N}$ NMR relaxation study

Sarata C. Sahu<sup>a</sup>, Abani K. Bhuyan<sup>b</sup>, Jayant B. Udgaonkar<sup>b</sup> & R.V. Hosur<sup>a,\*</sup>

<sup>a</sup>Department of Chemical Sciences, Tata Institute of Fundamental Research, Homi Bhabha Road, Mumbai 400005, India; <sup>b</sup>National Centre for Biological Sciences, Tata Institute of Fundamental Research, University of Agricultural Sciences (UAS) - Gandhi Krishi Vigyan Kendra (GKVK) Campus, Bangalore 560 065, India

Received 18 April 2000; Accepted 7 July 2000

**Key words:** backbone dynamics, barnase, barstar, complex,  $^{15}\text{N}$  NMR relaxation, protein–protein interactions

### Abstract

Backbone dynamics of uniformly  $^{15}\text{N}$ -labeled free barnase and its complex with unlabelled barstar have been studied at 40 °C, pH 6.6, using  $^{15}\text{N}$  relaxation data obtained from proton-detected 2D  $\{^1\text{H}\}$ - $^{15}\text{N}$  NMR spectroscopy.  $^{15}\text{N}$  spin-lattice relaxation rate constants ( $R_1$ ), spin-spin relaxation rate constants ( $R_2$ ), and steady-state heteronuclear  $\{^1\text{H}\}$ - $^{15}\text{N}$  NOEs have been measured at a magnetic field strength of 14.1 Tesla for 91 residues of free barnase and for 90 residues out of a total of 106 in the complex (excluding three prolines and the N-terminal residue) backbone amide  $^{15}\text{N}$  sites of barnase. The primary relaxation data for both the cases have been analyzed in the framework of the model-free formalism using both isotropic and axially symmetric models of the rotational diffusion tensor. As per the latter, the overall rotational correlation times ( $\tau_m$ ) are 5.0 and 9.5 ns for the free and complexed barnase, respectively. The average order parameter is found to be 0.80 for free barnase and 0.86 for the complex. However, the changes are not uniform along the backbone and for about 5 residues near the binding interface there is actually a significant decrease in the order parameters on complex formation. These residues are not involved in the actual binding. For the residues where the order parameter increases, the magnitudes vary significantly. It is observed that the complex has much less internal mobility, compared to free barnase. From the changes in the order parameters, the entropic contribution of NH bond vector motion to the free energy of complex formation has been calculated. It is apparent that these motions cause significant unfavorable contributions and therefore must be compensated by many other favorable contributions to effect tight complex formation. The observed variations in the motion and their different locations with regard to the binding interface may have important implications for remote effects and regulation of the enzyme action.

**Abbreviations:** 2D, two-dimensional;  $R_1$  ( $= 1/T_1$ ), spin-lattice relaxation rate;  $R_2$  ( $= 1/T_2$ ), spin-spin relaxation rate; NOE, nuclear Overhauser effect;  $S^2$ , generalized order parameter;  $\tau_m$ , overall rotational correlation time;  $\tau_e$ , effective correlation time for internal motions;  $R_{ex}$ , exchange contribution to line shape;  $\omega$ , Larmor frequency;  $D$ , diffusion constant; CSA, chemical shift anisotropy; HSQC, heteronuclear single quantum coherence.

### Introduction

Specific protein–protein interactions have been known for a long time to be of primary importance for many biological functions inside a living cell. A substantial understanding of these interactions has been obtained

during the past decades, thanks to the possibility of determination of three-dimensional structures of macromolecules and their complexes by physical techniques such as X-ray crystallography and NMR. This knowledge has led further to the design of molecules with altered functions as per one's desire. While the information on three-dimensional structures of macromolecules has thrown light on the finer details of the

\*To whom correspondence should be addressed. E-mail: jayant@ncbs.res.in; hosur@tifr.res.in

interactions between them, it is envisaged that many of the regulatory functions and enzyme mechanisms may have subtle dependence on their dynamical properties (Kim et al., 1998). Now, it is well known that proteins have various motions covering a wide range of amplitudes and time-scales ranging from picoseconds to hours. These movements may correlate with protein function, e.g. enzyme action (Epstein et al., 1995), protein-protein interaction (Carr et al., 1997), protein-ligand interaction (Fushman et al., 1994; Stivers et al., 1996; Hodsdon and Cistola, 1997) and protein-DNA interactions (Lefèvre et al., 1996; Slijper et al., 1997; Werten et al., 1999), etc., but the relative contributions of the various motions to function are yet to be known. Therefore, it is anticipated that detailed investigations of dynamics of proteins may provide better insights into the fundamental relationship between protein structure and function.

In the above respect NMR offers a great advantage over all the other techniques and enables detailed characterization of sequence specific local and global dynamical properties of proteins in aqueous solution. Heteronuclear  $^{15}\text{N}$  and  $^{13}\text{C}$  relaxation studies have thus been used extensively during the last few years to characterise the backbone/side-chain dynamics and motional properties of many protein molecules (Palmer et al., 1996; Kay, 1998; Malmendal et al., 1999; Prompers et al., 1999, Ye et al., 1999). Although the physical concepts and the techniques for the interpretation of relaxation data are evolving taking into consideration the shapes and isotropic or anisotropic motions of the molecules (Tjandra et al., 1997), the analyses have proved successful in providing qualitative trends in the local behaviors and these are expected to be of great help in understanding enzyme functions (Epstein et al., 1995; Mine et al., 1999).

*Barnase* is an extracellular ribonuclease with 110 amino acid residues and its enzyme action is inhibited by a protein, barstar, which has 89 residues. For both proteins crystal as well as solution structures are known (Mauguen et al., 1982; Bycroft et al., 1991; Lubienski et al., 1994). Barnase has two N-terminal  $\alpha$ -helices and a five-stranded anti-parallel  $\beta$ -sheet. The main hydrophobic core is formed by the packing of the first  $\alpha$ -helix against the  $\beta$ -sheet. On the other side of the  $\beta$ -sheet a broad shallow groove runs along almost the entire length of the molecule. Residues His-102, Glu-73 and Arg-87, which are strictly conserved within the family of ribonucleases, are located in the shallow groove and form the active site. Barnase rapidly forms a tight 1:1 complex ( $K_d = 10^{-14}\text{M}$ )

with barstar on mixing the two components and this complex is stable for a long period of time (Jones et al., 1993). A 2.6 Å resolution X-ray structure of the complex of barnase with the barstar double mutant C40,82/A (Guillet et al., 1993) gave the first description of the barstar fold and structural details of its interaction with barnase. The inhibitor, barstar, was found to bind the enzyme in the shallow groove of the enzyme. Extensive protein folding studies have been carried out on wild type and mutant systems of this enzyme and the relative stabilities of the various mutants have been investigated (Matouschek et al., 1992). The thermodynamics of folding has been studied and the intermediates in the folding pathways have been identified (Fersht, 1993). Protein engineering studies have shown that barnase contains two nucleation sites for folding, situated in the first helix and in the  $\beta$ -pleated sheet (Arcus et al., 1995; Freund et al., 1996). Fersht has described the folding of barnase as a process in which two foldons form independently and form a stable intermediate (Fersht, 1997). At high protein concentrations and acidic conditions the association of foldons from different monomers becomes more favorable, resulting in stable oligomers (Sanz et al., 1994). However, we observed that detailed dynamics studies on this system are lacking. In view of this we report here a comparative study of the internal dynamics of barnase and its complex with its specific inhibitor barstar. To our knowledge this is the first report on the backbone dynamics of a protein when it is bound to another protein, of approximately equal size. Our results reveal that the enzyme has a fairly rigid structure and, on average, the rigidity increases on complex formation. We also see some interesting changes near the active site and also in other locations along the polypeptide backbone.

## Materials and methods

### *$^{15}\text{N}$ labeling and sample preparation*

For *barnase* the efficient method of overproduction and purification as described by Okorokov et al. (1994) was followed.  $^{15}\text{N}$  labeling was achieved by growing the cells in minimal M9 media containing  $^{15}\text{NH}_4\text{Cl}$  (1 g/l) as the sole source of nitrogen. Final purification was done by FPLC using a Resource S column loaded in 50 mM ammonium acetate buffer, pH 4.5 and eluted by a gradient of ammonium acetate buffer, pH 8.0. The yield of U- $^{15}\text{N}$  barnase was

15 mg per liter of minimal medium. Unlabelled barstar purification was as given by Khurana et al. (1994) and the yield was 100 mg from a liter of culture. The complex was prepared by titrating U- $^{15}\text{N}$  barnase with unlabelled barstar to reach a final ratio of 1:1.2. The formation of the complex was monitored by recording  $^{15}\text{N}$ - $^1\text{H}$  HSQC spectra at different stages of titration. The peak due to N58 shifts substantially ( $\sim 1.35$  ppm in  $\text{H}^{\text{N}}$  chemical shift) on complex formation (Jones et al., 1993). The extinction coefficients of barstar and barnase are 20 200 and 22 100  $\text{M}^{-1} \text{cm}^{-1}$ , respectively (Fitzgerald and Hartley, 1993) and the concentrations of barstar and barnase were measured from the O.D. at 280 nm.

#### *NMR measurements*

For NMR experiments, 600  $\mu\text{l}$  of 2 mM  $^{15}\text{N}$ -enriched barnase and complex were prepared separately in 20 mM sodium phosphate buffer, pH 6.6, containing 10%  $\text{D}_2\text{O}$ . All NMR experiments were done at 40 °C on a Varian Unity plus spectrometer operating at a  $^1\text{H}$  frequency of 600.051 MHz, equipped with a Performa II pulsed field gradient unit and an actively shielded triple resonance z-gradient probe. For both the samples relaxation measurements were performed by recording  $R_1$ ,  $R_2$  and NOE relaxation spectra according to the established methods (Kay et al., 1989; Skelton et al., 1993; Farrow et al., 1994), which use pulsed field gradients for coherence transfer pathway selection combined with sensitivity enhancement (Cavanagh et al., 1991; Palmer et al., 1991). Quadrature detection along the indirectly detected dimension was achieved by the States-TPPI method (Marion et al., 1989).  $R_1$  and  $R_2$  HSQC spectra were recorded as  $90 \times 2048$  complex matrices with 16 scans per complex  $t_1$  point and spectral widths of 2000 and 9000 Hz along the  $\omega_1$  and  $\omega_2$  dimensions, respectively. A recycle delay of 1.5 s (including the acquisition time) was used for  $R_1$  and  $R_2$  measurements. For  $R_1$  measurement, spectra were recorded with 8 inversion recovery delays in the range 36 ms to 1296 ms and  $R_2$  spectra were recorded at 7 CPMG delays in the range from 15 ms to 191 ms. The spectra were duplicated at three different time points for each measurement as indicated by  $\times 2$  (see below). The 8 inversion recovery delays were: 36 ms, 77 ms ( $\times 2$ ), 178 ms, 296 ms ( $\times 2$ ), 397 ms, 598 ms, 799 ms ( $\times 2$ ) and 1296 ms.  $^1\text{H}$   $180^\circ$  pulses were inserted during the inversion recovery times and CPMG delays to eliminate the effects of cross relaxation and cross correlation as described

previously (Palmer et al., 1991; Farrow et al., 1994; Peng et al., 1994). In the CPMG experiments, the delay ( $\tau$ ) between the  $180^\circ$  pulses was 550  $\mu\text{s}$ . The 7 CPMG delays for  $R_2$  measurement were 15 ms ( $\times 2$ ), 31 ms, 46 ( $\times 2$ ) ms, 78 ms, 115 ( $\times 2$ ) ms, 138 ms and 191 ms.  $\{^1\text{H}\}$ - $^{15}\text{N}$  NOE spectra of  $80 \times 2048$  complex matrices with 48 scans for each complex  $t_1$  point were recorded with and without proton saturation during the relaxation delay. Spectral widths along the  $\omega_1$  and  $\omega_2$  dimensions were the same as used in  $R_1$  and  $R_2$  measurements. A recycle delay of 6 s was used for the spectrum recorded in the absence of proton saturation, whereas a 3 s recycle delay followed by a 3 s period of proton saturation was used with the NOE experiment.  $^1\text{H}$  saturation was achieved with a burst of  $120^\circ$   $^1\text{H}$  pulses at 5 ms intervals (Peng and Wagner, 1994).

#### *Data processing*

All spectra were processed using FELIX 95.0 (Biosym Technologies). To improve resolution, spectra were linear-predicted to twice the number of acquired points along the  $\omega_1$  dimension prior to Fourier transformation. All spectra were zero-filled to 1024 complex points along  $\omega_1$  and 4096 complex points along  $\omega_2$ . Resolution enhancement was achieved by applying a Lorentz-Gauss window along  $\omega_2$  and a  $60^\circ$ -shifted sine square bell function along  $\omega_1$ . The final sizes of the matrices were 2048 ( $\omega_2$ )  $\times$  1024 ( $\omega_1$ ). Most of the peaks were well resolved for peak height measurements (Skelton et al., 1993).

#### *$^{15}\text{N}$ relaxation parameters ( $R_1$ , $R_2$ , and NOE)*

Intensities (in arbitrary units) for the amide  $^{15}\text{N}$ - $^1\text{H}$  cross peaks were determined by measuring the heights of the peaks using FELIX software. Uncertainty in the peak height was measured from the duplicate spectra and this was extrapolated to the remaining time points. After obtaining peak heights and their errors, the above time series was fitted to a single exponential decay function:

$$I(t) = A + B e^{-R_{1,2}t} \quad (1)$$

where  $I(t)$  is the intensity (obtained from peak height measurements) at recovery delay  $t$  (ms),  $A + B$  is the intensity at time  $t = 0$ , and  $A$  is the steady state value which is the intensity at  $t = \infty$ . Errors in  $R_1$  and  $R_2$  were estimated as standard errors from the Levenberg-Marquardt fitting routine.

The  $\{^1\text{H}\}$ - $^{15}\text{N}$  heteronuclear NOE was calculated from the equation:

$$\text{NOE} = \frac{I_{\text{sat}}}{I_{\text{eq}}}, \quad (2)$$

where  $I_{\text{sat}}$  and  $I_{\text{eq}}$  are the intensities of a peak from the spectra collected with and without proton saturation, respectively. Next, two duplicate spectra were analyzed in a similar way (i.e., Equation 2) to derive the uncertainty of the measurement.

### Model free analysis

The major sources of relaxation for amide  $^{15}\text{N}$  nuclear spins in proteins are dipolar coupling with the attached proton, and anisotropy of the  $^{15}\text{N}$  chemical shift. The movement of the NH bond axis is characterized by the spectral density function  $J(\omega)$ , which is related to three parameters that describe the relaxation of the  $^{15}\text{N}$  spin: the longitudinal relaxation rate ( $R_1$ ), the transverse relaxation rate ( $R_2$ ), and the steady-state NOE enhancement ( $\eta$ ) (Abragam, 1961). The relaxation parameters of  $^{15}\text{N}$  are related to  $J(\omega)$ , at five different frequencies by the following equations.

$$R_1 = \frac{1}{4}d^2\{J(\omega_H - \omega_N) + 3J(\omega_N) + 6J(\omega_H + \omega_N)\} + c^2J(\omega_N) \quad (3)$$

$$R_2 = \frac{1}{8}d^2\{4J(0) + J(\omega_H - \omega_N) + 3J(\omega_N) + 6J(\omega_H) + 6J(\omega_H + \omega_N)\} + \frac{c^2}{6}\{4J(0) + 3J(\omega_N)\} + R_{\text{ex}} \quad (4)$$

$$\text{NOE} = \frac{d^2}{4R_1} \frac{\gamma_H}{\gamma_N} \{6J(\omega_H + \omega_N) - J(\omega_H - \omega_N)\} + 1 \quad (5)$$

where

$$d = \frac{\mu_0}{4\pi} \gamma_H \gamma_N \frac{h}{2\pi} (r_{\text{NH}}^{-3}) \quad (6)$$

$$c = \omega_N (\sigma_{\parallel} - \sigma_{\perp}) / \sqrt{3} \quad (7)$$

where  $\mu_0$  is the permeability of the free space,  $\gamma_H$  and  $\gamma_N$  are the gyromagnetic ratios of  $^1\text{H}$  and  $^{15}\text{N}$  ( $2.6752 \times 10^8$  and  $-2.712 \times 10^7$  rad s $^{-1}$  T $^{-1}$ , respectively);  $\omega_H$  and  $\omega_N$  are the Larmor frequencies of  $^1\text{H}$  and  $^{15}\text{N}$  respectively,  $r_{\text{NH}}$  is the N-H bond length (taken here to be 1.02 Å) and  $J(\omega_i)$  are the spectral densities at the angular frequency  $\omega_i$ . An axially symmetric chemical shift tensor has been assumed for  $^{15}\text{N}$  with  $\sigma_{\parallel} - \sigma_{\perp} = -160$  ppm (Hiyama et al., 1988).

$R_{\text{ex}}$  has been included in Equation 4 to accommodate chemical exchange and other pseudo-first-order processes that contribute to the decay of transverse magnetization (Bloom et al., 1965). The  $R_{\text{ex}}$  term in Equation 4 represents line broadening due to chemical exchange and/or conformational averaging on a time scale slower than the overall rotational correlation time,  $\tau_m$ . This is actually treated as a variable and adjusted to fit the experimental data (see later).

The amplitudes and effective correlation times of the internal motions of a protein are determined from the relaxation data by using the model-free formalism pioneered by Lipari and Szabo (1982a,b) and extended by Clore et al. (1990a, b). In this analysis, the spectral density function,  $J(\omega)$ , is modeled differently depending upon whether the rotational diffusion tensor is isotropic or anisotropic. In the former case, as per the modification by Clore (Clore et al., 1990b) when the internal motions of the NH bond are considered to occur on two fast but significantly different time scales characterized by two effective correlation times,  $\tau_f$  and  $\tau_s$ , with  $\tau_f \ll \tau_s \ll \tau_m$  (Clore et al., 1990b),

$$J(\omega) = \frac{2}{5} \left[ \frac{S^2 \tau_m}{1 + (\omega \tau_m)^2} + \frac{(1 - S_f^2) \tau_f'}{1 + (\omega \tau_f')^2} + \frac{(S_f^2 - S^2) \tau_s'}{1 + (\omega \tau_s')^2} \right] \quad (8)$$

in which,

$$\frac{1}{\tau_f'} = \frac{1}{\tau_f} + \frac{1}{\tau_m} \quad (9)$$

$$\frac{1}{\tau_s'} = \frac{1}{\tau_s} + \frac{1}{\tau_m} \quad (10)$$

where  $S^2 = S_f^2 S_s^2$  is the square of the generalized order parameter characterizing the amplitude of internal motions of each NH bond, and  $S_f^2$  and  $S_s^2$  are the squares of the order parameters for the internal motions on the fast and slower time scales, respectively. The model-free spectral density function in Equation 8 assumes that the overall tumbling motion of the molecule is isotropic. Motions represented by the generalized order parameter will be referred to as dynamics on the ps to ns time scale. The order parameter specifies the degree of spatial restriction of the NH bond. Assuming that the motion of the NH bond

can be described by diffusion in a cone of semiangle  $\theta$ ,  $S^2$  is given by:

$$S^2 = \frac{\cos^2 \theta (1 + \cos \theta)^2}{4} \quad (11)$$

Thus,  $S^2 = 0$  ( $\theta = \pi/2$ ), for isotropic internal motions, and  $S^2 = 1$  ( $\theta = 0$ ), for no motion.

For the situation when the rotational diffusion tensor is anisotropic, more complicated expressions have been described (Schurr et al., 1994; Tjandra et al., 1995; Zheng et al., 1995; Fushman et al., 1997). However, for the case of an axially symmetric tensor, simplifications occur and the spectral density function is approximated, for the situations when the internal motions are much faster than the overall tumbling rate (Tjandra et al., 1995), as:

$$J(\omega) = \frac{2}{5} \left[ S^2 \sum_{k=1}^3 \frac{A_k \tau_k}{1 + (\omega \tau_k)^2} + \frac{(1 - S^2) \tau}{1 + (\omega \tau)^2} \right] \quad (12)$$

where  $A_1 = (1.5 \cos^2 \alpha - 0.5)^2$ ,  $A_2 = 3 \sin^2 \alpha \cos^2 \alpha$ , and  $A_3 = 0.75 \sin^4 \alpha$ .

$\alpha$  is the angle between the NH bond vector and the unique axis of the principal frame of the diffusion tensor,  $\tau_1 = (6D_{\perp})^{-1}$ ,  $\tau_2 = (D_{\parallel} + 5D_{\perp})^{-1}$ ,  $\tau_3 = (4D_{\parallel} + 2D_{\perp})^{-1}$  and  $\tau^{-1} = 6D + \tau_e^{-1}$  where  $D$  is  $\frac{1}{3}$  the trace of the diffusion tensor,  $D_{\parallel}$  and  $D_{\perp}$  are the components of the axially symmetric diffusion tensor, parallel and perpendicular to the axis of symmetry, respectively. The isotropic correlation time  $\tau_m$  is related to  $D$  by the equation:  $\tau_m = (6D)^{-1}$ . We have carried out the analysis of the relaxation data using both the approaches.

#### *Dynamical model selection and parameter estimation*

For selection of a dynamical model describing internal motion, in a residue specific manner, and to estimate the involved parameters for a model, the procedure described by Mandel et al. (1995) was followed. In this exercise, the spectral densities for the isotropic and axially symmetric diffusion tensors would be of course different. Those for the axially symmetric case for different models are given in Table 1. In the first stage, the best model for a residue was selected by fitting the experimental data to the different models separately and the one with the minimum number of parameters was preferred. After selecting the best model in this manner  $\tau_m$  was optimized along with the other model parameters, again using the grid search method. All

optimization involved minimization of the  $\chi^2$  function (Mandel et al., 1995):

$$\chi^2 = \sum_i^n \Gamma_i = \sum_i^n \sum_j^{m_j} (E_{ij} - S_{ij})^2 / \sigma_{ij}^2 \quad (13)$$

where the index  $i$  refers to an amide  $^{15}\text{N}$  site with  $N$  being the total number of sites, and  $\Gamma_i$  is the sum-squared error for site  $i$ .  $m_j$  represents the number of experimentally determined relaxation parameters for the  $i$ th site.  $E_{ij}$ ,  $S_{ij}$ , and  $\sigma_{ij}$ , respectively, are experimental relaxation parameters, simulated relaxation parameters, and the experimental uncertainty in the  $j$ th relaxation parameter.

The model calculations were performed using the program model-free (version 4.1) provided by Dr Arthur G. Palmer, which has the options for choosing the model describing rotational diffusion. To determine random error in the model free parameters arising from experimental uncertainties, 500 simulated data sets were generated by Monte Carlo simulation, assuming that the standard errors in the measured relaxation parameters follow Gaussian distributions.

## **Results**

### *$^{15}\text{N}$ assignments*

Figure 1 shows illustrative 2D  $\{^1\text{H}-^{15}\text{N}\}$  HSQC spectra of barnase (a) and its complex with barstar (b) at 313 K, pH 6.6 used to measure  $^{15}\text{N}$  relaxation data. The assignments indicated for the 106 residues of barnase are mostly as per those reported by Jones et al. (1993). But since the dispersion of peaks is better at 600 MHz (for  $^1\text{H}$ ) spectrometer frequency, some of the ambiguities in the reported assignments were removed by analysing  $^{15}\text{N}$ -edited TOCSY-HSQC and NOESY-HSQC spectra of barnase. Following these assignments, 91  $^1\text{H}-^{15}\text{N}$  non-overlapping peaks have been identified in the fingerprint region of the HSQC spectra, a sample of which is shown in Figure 1a. Similarly for the complex, initial assignments were obtained by comparison with the published spectra (Jones et al., 1993). S85, which was not assigned in the complex, was assigned by elimination at the first stage for the assignment of the complex. Subsequently all the assignments were confirmed by the concerted use of  $^{15}\text{N}$ -edited TOCSY-HSQC and NOESY-HSQC spectra. An HSQC spectrum of the complex with the assignments is shown in Figure 1b.

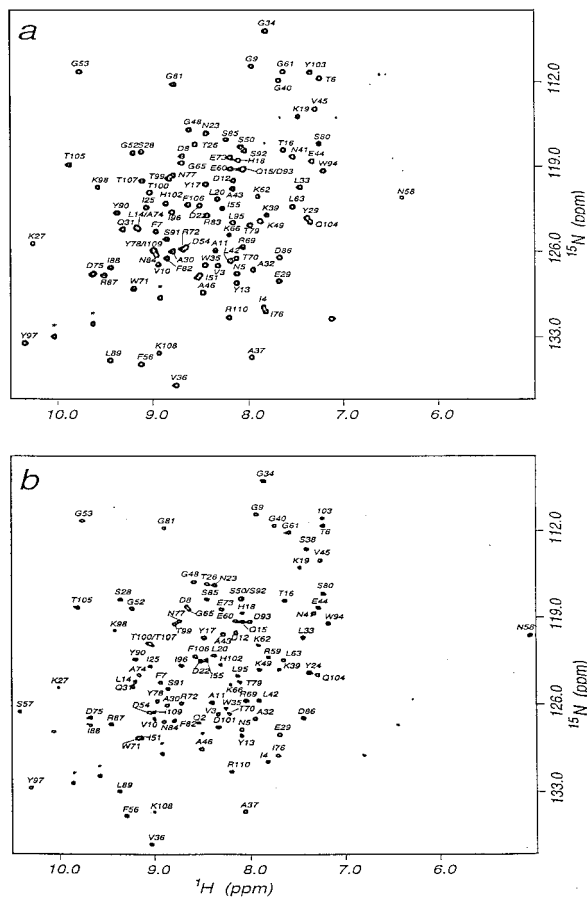


Figure 1. A portion of the  $^1\text{H}$ - $^{15}\text{N}$  HSQC 2D NMR spectrum of (a) barnase and (b) its complex with the polypeptide inhibitor barstar at pH 6.6, 40 °C. The peaks marked \* are from side-chain indole  $^{15}\text{N}$ - $^1\text{H}$  correlations and are excluded from the analysis.

### $^{15}\text{N}$ $R_1$ , $R_2$ , and $\{^1\text{H}$ - $^{15}\text{N}\}$ NOE

To obtain the primary relaxation data the non-overlapping cross peaks were analyzed by peak height measurements. The backbone  $^{15}\text{N}$   $R_1$ ,  $R_2$  and NOE could be measured for 91 and 90 non-overlapping residues in the case of barnase and the complex, respectively. For the rest of the residues in both barnase and complex the relaxation parameters could not be measured either due to overlap of peaks or the intensities of the peaks were very low for reliable measurement of the peak heights.

The calculated  $R_1$ ,  $R_2$  values, and the NOEs for 91 backbone  $^{15}\text{N}$  sites in case of barnase and 90 for the complex are shown in Figure 2. Filled and open circles are the data for barnase and the complex respectively. Also two tables comprising the  $R_1$ ,  $R_2$ , and the NOEs for both barnase and complex, are available as sup-

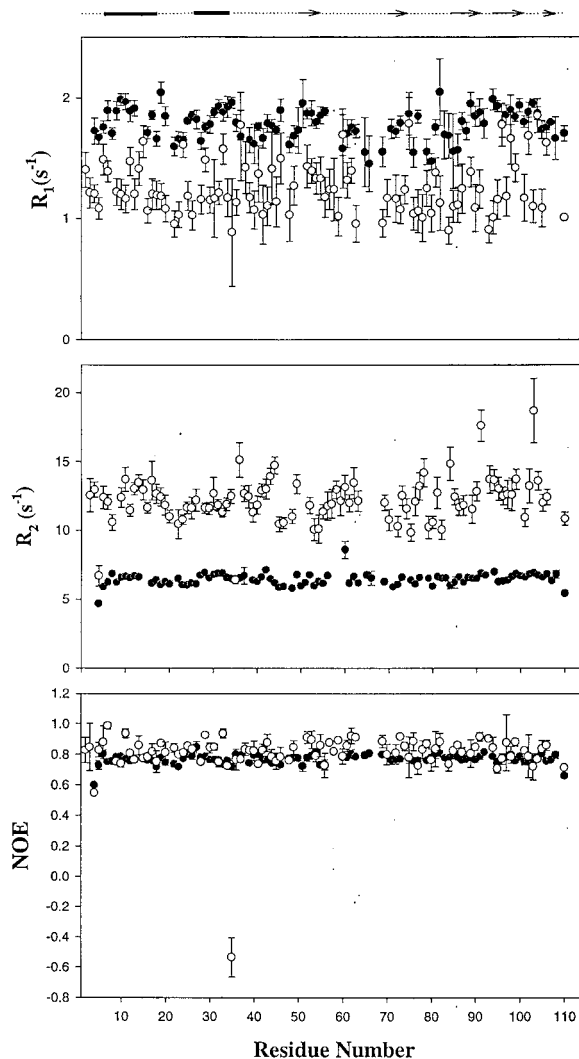


Figure 2. Relaxation parameters for barnase and its complex with barstar. The values of  $R_1$ ,  $R_2$ , and proton-irradiated NOE for individual residues are shown as a function of residue number in the protein sequence. The filled and open circles are for barnase and the complex respectively. Errors in the measured relaxation parameters are also shown. The  $\alpha$ -helices and  $\beta$ -strands are depicted as thick lines and arrows respectively at the top of the figure.

porting material (Tables S1 and S2, respectively). We notice that, on average, the  $R_2$  and NOE values increase, whereas  $R_1$  decreases upon complex formation. The average values of  $R_2$  and NOE increase by  $\sim 89\%$  (ca. from 6.445 to 12.181) and  $\sim 5.0\%$  (ca. from 0.770 to 0.81) respectively, whereas the average value of  $R_1$  decreases by  $\sim 30\%$  (ca. from 1.778 to 1.248). It can also be noted that although there is an increase/decrease in the average values, the trend is not

similar along the backbone and the extent of variation is different for different residues.

*Model free analysis of relaxation parameters ( $R_1$ ,  $R_2$ , and NOE)*

From the point of view of quantitative interpretation of relaxation data (Figure 2), there has been extensive discussion in the recent literature on the analysis of such commonly available three relaxation parameters in terms of the dynamical variables (Beeser et al., 1997; Fischer et al., 1997; Luginbühl et al., 1997; Kroenke et al., 1998; Vis et al., 1998; Bhattacharya et al., 1999; Lee et al., 1999; LeMaster, 1999; Prompers et al., 1999). The dynamical variables include the order parameters ( $S^2$ ), the internal correlation time ( $\tau_e$ ), the global rotational correlation time ( $\tau_m$ ), and conformational or chemical exchange rates ( $R_{ex}$ ). A commonly used approach for this purpose is the ‘Model-free analysis’ whose details have been discussed in Materials and methods. It is a phenomenological approach, involves certain types of assumptions with regard to frequency, symmetry and amplitudes of motions and the bottom line is to fit the experimental data and obtain useful information about the system. If the rotational diffusion is anisotropic and if this is not included in the analysis, erroneous conclusions would be derived for the exchange rates. The errors introduced have been estimated by fitting simulated data and it is observed that for a rigid non-spherical body,  $R_2$  is underestimated by 20% for anisotropies with  $D_{||}/D_{\perp}$  equal to 2.0 (Tjandra et al., 1997). For moderate anisotropies, estimates of order parameters may be tolerant to the assumptions of isotropic motions, but the internal correlation times ( $\tau_f$  and  $\tau_s$ ) may be over-estimated (Luginbühl et al., 1997; Tjandra et al., 1997) and the exchange contribution may be artificial, since both conformational exchange and anisotropic motion contribute to the measured  $R_2$  values.

The  $^{15}\text{N}$   $R_2/R_1$  ratio is to a good approximation independent of rapid internal motions and of the magnitude of the chemical shift anisotropy. Therefore it provides a good measure of the global tumbling rate of the NH vectors. Residues with large-amplitude internal motions on a time scale longer than a few hundred picoseconds which can be identified by low NOE values, must be excluded from this analysis. In addition, the residues which satisfy the condition,

$$\frac{(\langle T_2 \rangle - T_{2,n}) / \langle T_2 \rangle}{-((T_1) - T_{1,n}) / \langle T_1 \rangle} > 1.5SD, \quad (14)$$

where SD is the standard deviation of the left hand side, also must be excluded from the above calculation, since these are likely to have conformational exchange contributions to the  $T_2$  values. Following the above procedures, the mean  $R_2/R_1$  ratios were found to be  $3.7 \pm 0.3$  and  $10.2 \pm 1.3$  for free barnase and complex, respectively. From these  $R_2/R_1$  ratios the initial estimates of  $\tau_m$  were found to be  $5.20 \pm 0.29$  ns and  $9.79 \pm 0.69$  ns, for barnase and complex, respectively. These values were optimised later (Mandel et al., 1995). From the reported structural data of barnase (1bnr.pdb) and of complex (1brs.pdb), initial estimates of the principal components of the inertial tensors for barnase and the complex were derived to be 1.0:0.87:0.56 and 1.0:0.90:0.56, respectively. These values vary significantly from a sphere. The asymmetry was further verified using the program R2R1\_1.1. The program indicates a statistically better fit for the relaxation data ( $R_2/R_1$  ratios here) using an axially symmetric model over an isotropic model with the values for  $\tau_m$ ,  $D_{||}/D_{\perp}$ ,  $\theta$  and  $\phi$  as 5.01 ns, 1.09, 0.75 and 1.09 respectively for free barnase and 9.13 ns, 1.20, 1.22 and 0.23 respectively for the complex. Further, for both the cases no significant improvement in the fully anisotropic model over axially symmetric diffusion has been observed.

Starting from the above initial estimates of  $\tau_m$ ,  $D_{||}/D_{\perp}$ ,  $\theta$  and  $\phi$ , we analysed the  $^{15}\text{N}$  relaxation data residuewise using both the isotropic and axially symmetric models for rotational diffusion tensor as described in Materials and methods. The parameters were iteratively refined along with  $S^2$  and  $\tau_e$  parameters to fit the  $^{15}\text{N}$ ,  $R_1$ ,  $R_2$  and NOE data according to the model selection procedure described by Mandel et al. (1995). This comparative study of isotropic vs axially symmetric models for rotational diffusion, yielded the following results:

- (i) In going from the isotropic to the axially symmetric case, the average order parameters changed from 0.78 to 0.80 for free barnase and for the complex the value of 0.86 did not change. It is interesting to note that, despite the larger anisotropy of rotational diffusion in the complex ( $D_{||}/D_{\perp} = 1.26$ ), there is less effect on the derived order parameters.
- (ii) Conformational exchange was necessary in the isotropic case for about 5 residues, whereas it was completely absent in the axially symmetric case.
- (iii) The results with respect to the contribution of  $\tau_e$  were nearly similar in both the cases.

Table 1. Model-free spectral density functions used during the analysis.

Model	Spectral density function
1*	$J(\omega) = \frac{2}{5} \left[ S^2 \sum_{k=1}^3 \frac{A_k \tau_k}{1 + (\omega \tau_k)^2} \right]$
2*	$J(\omega) = \frac{2}{5} \left[ S^2 \sum_{k=1}^3 \frac{A_k \tau_k}{1 + (\omega \tau_k)^2} + \frac{(1 - S^2)\tau}{1 + (\omega \tau)^2} \right]$

\*Model 3 and 4 are derived from Models 1 and 2 by explicitly including  $R_{ex}$  in the definition of  $R_2$ , as an optimizable parameter. In Model 1,  $S^2$  and  $\tau_m$  are the optimized parameters and in Model 2,  $S^2$ ,  $\tau_m$  and  $\tau_e$  are optimized.

Keeping in mind the observation that the rotational diffusion tensor is not isotropic, and the axially symmetric tensor yielded a better fit to the relaxation data, we discuss below the results obtained for the free barnase and the complex, only for the axially symmetric case. The final optimised parameters for  $\tau_m$  and  $D_{\parallel}/D_{\perp}$  for barnase and complex were (4.99 ns, 1.1) and (9.46 ns, 1.26) respectively. The values of  $\theta$  and  $\phi$  were  $-44.5 \pm 1.0$  and  $52.3 \pm 1.1$  respectively for barnase and  $-37.1 \pm 2$  and  $33.1 \pm 2.5$ , respectively, for the complex. All the data could be fitted with the dynamical models, Model 1 or Model 2 (see Table 1). Model 1, in which  $S^2$  is the sole fitting parameter, best described the data for 73 NH vectors in the complex and 51 vectors in free barnase. Model 2, for which  $S^2$  and  $\tau_e$  are the parameters, best described the relaxation of 16 NH vectors in the complex and 40 vectors in free barnase. The model-free parameters thus obtained are plotted in Figure 3. Tables listing these values are also supplied in the supporting information (see Tables S3 and S4) and some of these parameters are described below.

### Dynamic changes induced by complex formation

#### Overall rotational correlation time ( $\tau_m$ )

The optimized value of  $\tau_m$  was  $4.99 \pm 0.03$  ns in free barnase and this increased to  $9.46 \pm 0.09$  ns after complex formation with barstar. This must be expected considering that the complex is almost twice as massive as the free protein. The measured values are reasonable for the sizes of the two systems (barnase  $\sim 12$  kDa and barnase-barstar complex  $\sim 22$  kDa).

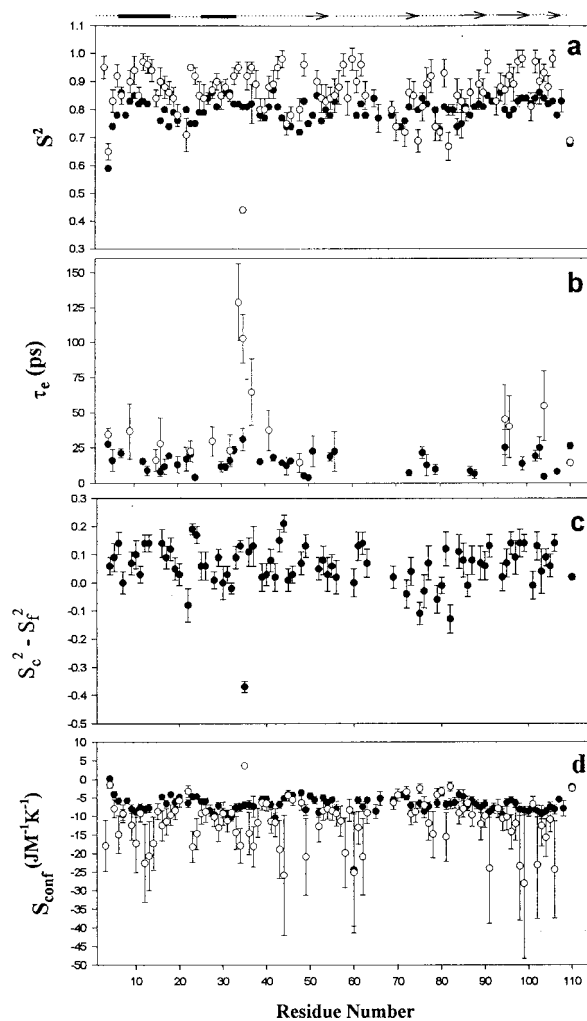


Figure 3. Parameters defining the dynamics of barnase and its complex with barstar. The order parameter,  $S^2$  (a), the internal correlation time,  $\tau_e$  (b), the difference in  $S^2$  between the complex and free barnase (c) and conformational entropy (d) for each amino acid residue along with the errors are plotted as a function of residue number in the protein sequence. Wherever both filled and open circles are present, the filled circles are for barnase and open circles are for the complex. The  $\alpha$ -helices and  $\beta$ -strands are depicted as thick lines and arrows, respectively, at the top of the figure.

#### The distribution of $S^2$

The average values of  $S^2$  in free and complexed barnase are 0.80 and 0.86, respectively. This shows an overall increase in  $S^2$  upon complex formation, and suggests greater rigidity of NH vectors in the complex as compared to that in free barnase. But as can be seen from Figure 3 there are residewise differences in the order parameters of the complexed and free barnase all along the barnase backbone. It is interesting to note



Figure 4. Ribbon diagram of barnase-barstar (C40,82/A) complex based on the crystal structure (1brs.pdb). In barnase, the residues for which  $S^2$  increases upon complex formation are shown as red, the residues for which  $S^2$  decreases are shown as green, the residues for which there is no significant change in  $S^2$  are shown in yellow and cyan indicates those residues for which data is not available.

that for about 5 residues (D22, W35, D75, T79 and F82), there is a significant decrease in the order parameters upon complex formation. For 24 residues, there is no change and for 49 residues there is an increase in the order parameter. For the rest, the comparison was not possible due to non availability of data for both the systems. In this exercise, only those changes are considered significant which are larger than the root mean square error of 0.04 in the difference, calculated as

$$dS^2 = \frac{1}{N} \sum \left[ (dS_c^2)^2 + (dS_f^2)^2 \right]^{1/2}, \quad (15)$$

where  $N$  is the number of residues included in the calculation, which is 78. This information is shown in a color coded manner on the structure of the molecule in the complex in Figure 4. Significant increases in order parameters are seen for several residues in the regions 4–19, 23–29, 33–37 (35 actually shows a large decrease), 41–44, 48–53, 61–63, 84–91, and 95–106 (Figure 3 and Tables S3 and S4 of the supporting information). The first two of these are located in the N-terminal helical regions while the others form part of the  $\beta$ -sheets (Figure 3, top and Figure 4). The region 72–82 which shows a mixture of increases and decreases in the order parameters lies adjacent to the

binding interface. These order parameter changes of the different residues indicate, firstly, that the effects of barstar binding on the dynamics of barnase are not local in nature but extend also to other regions having different secondary structural characteristics (Figure 4), and secondly, the effects can be of different types. These observations are of significance and suggest possibilities of remote effects and relay of ligand perturbations.

Table 2 lists the residues at the binding surface of barnase with barstar and the order parameter changes therein. It is seen that for A37, N84–R87, H102, and Q104, there are significant increases in the order parameter on complex formation. On the other hand, for F56, E60 and T103 for which the data are available, the changes are insignificant. This may mean that the specific nature of the interactions of the residues contributes to the changes in the order parameters, i.e. there can be increase or decrease in the mobility of the NH vectors depending on the specific interactions.

#### Internal motion $\tau_e$

It is observed that internal motions in the complex are quite small (16 residues) as compared to free barnase (40 residues). Most of these are faster than 30 ps ex-

Table 2. Comparison of  $S^2$  of barnase residues interacting with barstar in free and complexed form

Residue	$S^2$ of free barnase	$S^2$ of complexed barnase	$dS^{2*}$
K27	0.84( $\pm$ 0.02)	–	
A37	0.82( $\pm$ 0.07)	0.95( $\pm$ 0.02)	0.13
S38	–	0.89( $\pm$ 0.05)	
F56	0.83( $\pm$ 0.01)	0.85( $\pm$ 0.06)	0.02
N58	–	0.96( $\pm$ 0.04)	
R59	–	0.84( $\pm$ 0.06)	
E60	0.98( $\pm$ 0.04)	0.98( $\pm$ 0.04)	0.0
R83	0.80( $\pm$ 0.02)	–	
N84	0.74( $\pm$ 0.03)	0.85( $\pm$ 0.06)	0.11
S85	0.75( $\pm$ 0.05)	0.83( $\pm$ 0.04)	0.08
R87	0.78( $\pm$ 0.01)	0.86( $\pm$ 0.05)	0.08
H102	0.84( $\pm$ 0.02)	0.97( $\pm$ 0.04)	0.13
T103	0.86( $\pm$ 0.01)	0.90( $\pm$ 0.08)	0.04
Q104	0.84( $\pm$ 0.01)	0.93( $\pm$ 0.03)	0.09

\* $dS^2$  is the difference in order parameters of complexed and free barnase.

cept for a few residues (34 and 35) in the complex, for which it is of the order of 100–130 ps. It is again interesting to note that the residues 34, 35 lying near the binding interface (residues A37, S38) get slowed down on complex formation.

#### Conformational entropy changes due to complex formation

Changes in the internal dynamics of protein molecules on complex formation have important consequences for the energetics of interaction, relay of information through the molecule, etc. Recently, a method has been described to relate the  $S^2$  values (Yang and Kay, 1996) to the conformational entropy arising out of ps time scale motion of the NH bond vectors. Assuming the bond motion to be confined to a cone, the following equation has been derived ( $S_{\text{conf}}$ )

$$S_{\text{conf}} = R \ln \pi [3 - (1 + 8S)^{0.5}], \quad (16)$$

where  $R$  is the gas constant and  $S$  is the square-root of the order parameter. The validity of the equation is limited to  $S^2 < 0.95$ . Residue-wise conformational entropy changes on complex formation have been calculated and these are shown in Figure 3 (bottom panel). It is observed that there are large changes in entropy on complex formation and this again varies along the polypeptide chain. Since an increase in the order parameter results in loss of entropy and vice versa, it follows that some residues lose entropy, some

gain and for others there is no significant change. Overall it turns out that complex formation leads to an entropic loss of free energy to the extent of roughly 81 kJ/mol at 40 °C. While this provides a useful feeling of NH vector motional contributions to free energy, intuitively the number looks rather too large for a tight binding complex. However, the above number cannot be taken to imply an overall entropic contribution to the free energy for the following reasons: (i) All the vectors in the molecule are not considered; (ii) The motions of the individual vectors are not necessarily independent while the formula assumes them to be so; (iii) The order parameters do not reflect motions outside the ns-ps time scale; (iv) Solvent ordering (disordering) is not included; (v) Corresponding changes due to barstar dynamics are not included. Now, for a binding constant of  $10^{14} \text{ M}^{-1}$  for the barnase-barstar complex, the total free energy change can be calculated to be  $(-RT \ln K) \sim -82 \text{ kJ/mol}$ . This implies that the loss of entropy due to internal ordering of the backbone bonds must be highly compensated by other factors such as H-bond interactions, hydrophobic interactions, solvent disordering etc. From Table 2, we notice that the residues involved in the interaction with barstar are largely polar type, implying (i) possibility of H-bond interaction including electrostatic interactions and (ii) increase in solvent entropy due to release of the ordered water molecules to the bulk on complex formation. Besides, structural changes away from the site of interaction are also conceivable – just

as there are order parameter changes at remote places, and these may also contribute to favorable free energy changes.

## Conclusions

We have described in this paper backbone dynamics of an enzyme barnase, in its free form and when it is bound to its inhibitor barstar. We have measured the  $^{15}\text{N}$  longitudinal, transverse and heteronuclear NOE relaxation parameters at a field strength of 14.1 Tesla and have analysed them using the model-free approach. The overall rotational correlation time of barnase was found to increase from  $\sim 5.0$  ns to  $\sim 9.5$  ns upon complexation with barstar, which is a consequence of increase in the molecular mass of the protein. On average there is an increase in the order parameters ( $S^2$ ) from 0.80 to 0.86, but the changes are quite varied along the backbone of barnase. A certain section of the protein, near the binding interface, shows a decrease in the order parameter on complex formation. Taken together, these observations are very interesting and suggest the possibility of remote effects on the interaction and relay of ligand perturbation. We have calculated the residue-wise conformational entropies from the respective backbone order parameters and these indicate that the NH vector motions on the ps-ns time scale make unfavorable entropic contributions to the binding process. This, however, does not represent the total entropic contribution and several other factors may be expected to be contributing favourably to the binding free energies.

## Acknowledgements

The NMR spectra were recorded at the National Facility for High Field NMR, TIFR, located at Mumbai, supported by the Department of Science and Technology, Government of India. We thank Dr. A. Majumdar, Prof. G. Govil and Prof. K.V.R. Chary for useful discussions.

## References

Abraham, A. (1961) *Principles of Nuclear Magnetism*, Clarendon Press, Oxford.  
 Arcus, V.L., Vuilleumier, S., Freund, S.M., Bycroft, M. and Fersht, A.R. (1995) *J. Mol. Biol.*, **254**, 305–321.  
 Beeser, S.A., Goldenberg, D.P. and Oas, T.G. (1997) *J. Mol. Biol.*, **269**, 154–164.

Bhattacharya, S., Falzone, C.J. and Lecomte, T.J. (1999) *Biochemistry*, **38**, 2577–2589.  
 Bloom, M., Reeves, L.W. and Wells, E.J. (1965) *J. Chem. Phys.*, **42**, 1615–1624.  
 Bycroft, M., Ludvigsen, S., Fersht, A.R. and Poulsen, F.M. (1991) *Biochemistry*, **30**, 8697–8701.  
 Carr, P.A., Erickson, H.P. and Palmer, A.G., III (1997) *Structure*, **5**, 949–959.  
 Cavanagh, J., Palmer, A.G., Wright, P.E. and Rance, M. (1991) *J. Magn. Reson.*, **91**, 429–436.  
 Clore, G.M., Szabo, A., Bax, A., Kay, L.E., Driscoll, P.C. and Gronenborn, A.M. (1990a) *J. Am. Chem. Soc.*, **112**, 4989–4991.  
 Clore, G.M., Driscoll, P.C., Wingfield, P.T. and Gronenborn, A.M. (1990b) *Biochemistry*, **29**, 7387–7401.  
 Epstein, D.M., Benkovic, S.J. and Wright, P.E. (1995) *Biochemistry*, **34**, 11037–11048.  
 Farrow, N.A., Muhandiram, R., Singer, A.U., Pascal, S.M., Kay, C.M., Gish, G., Shoelson, S.E., Pawson, T., Forman-Kay, J.D. and Kay, L.E. (1994) *Biochemistry*, **33**, 5984–6003.  
 Fersht, A.R. (1993) *FEBS Lett.*, **325**, 5–16.  
 Fersht, A.R. (1997) *Curr. Opin. Struct. Biol.*, **7**, 3–9.  
 Fischer, M.W.F., Zeng, L., Pang, Y., Hu, W., Majumdar, A. and Zwietering, E.R.P. (1997) *J. Am. Chem. Soc.*, **119**, 12629–12642.  
 Fitzgerald, P.C. and Hartley, R.W. (1993) *Anal. Biochem.*, **214**, 544–547.  
 Freund, S.M., Wong, K.B. and Fersht, A.R. (1996) *Proc. Natl. Acad. Sci. USA*, **93**, 10600–10603.  
 Fushman, D., Weisemann, R., Thüring, H. and Rüterjans, H. (1994) *J. Biomol. NMR*, **4**, 61–78.  
 Fushman, D., Cahill, S. and Cowburn, D. (1997) *J. Mol. Biol.*, **266**, 173–194.  
 Guillet, V., Laphorn, A., Hartley, R.W. and Mauguén, Y. (1993) *Structure*, **1**, 165–177.  
 Hiyama, Y., Niu, C.-H., Silverton, J.V., Bavoso, A. and Torchia, D.A. (1988) *J. Am. Chem. Soc.*, **110**, 2378–2383.  
 Hodsdon, M.E. and Cistola, D.P. (1997) *Biochemistry*, **36**, 2278–2290.  
 Jones, D.N.M., Bycroft, M., Lubienski, M.J. and Fersht, A.R. (1993) *FEBS Lett.*, **331**, 165–172.  
 Kay, L.E., Torchia, D.A. and Bax, A. (1989) *Biochemistry*, **28**, 8972–8979.  
 Kay, L.E. (1998) *Nat. Struct. Biol.*, **5** (NMR Supplement), 513–517.  
 Kim, H., Xia, D., Yu, C., Xia, J., Kachurin, A.M., Zhang, L., Yu, L. and Deisenhofer, J. (1998) *Proc. Natl. Acad. Sci. USA*, **95**, 8026–8033.  
 Khurana, R. and Udgaonkar, J.B. (1994) *Biochemistry*, **33**, 106–115.  
 Kroenke, C.D., Loria, J.P., Lee, L.K., Rance, M. and Palmer, A.G. III (1998) *J. Am. Chem. Soc.*, **120**, 7905–7915.  
 Lee, A.L., Flynn, P.F. and Wand, A.J. (1999) *J. Am. Chem. Soc.*, **121**, 2891–2902.  
 Lefèvre, J.-F., Dayie, K.T., Peng, J.W. and Wagner, G. (1996) *Biochemistry*, **35**, 2674–2686.  
 LeMaster, D.M. (1999) *J. Am. Chem. Soc.*, **121**, 1726–1742.  
 Lipari, G. and Szabo, A. (1982a) *J. Am. Chem. Soc.*, **104**, 4546–4559.  
 Lipari, G. and Szabo, A. (1982b) *J. Am. Chem. Soc.*, **104**, 4559–4570.  
 Lubienski, M.J., Bycroft, M., Freund, S.M.V. and Fersht, A.R. (1994) *Biochemistry*, **33**, 8866–8877.  
 Lugmühl, P., Pervushin, K.V., Iwai, H. and Wüthrich, K. (1997) *Biochemistry*, **36**, 7305–7312.

- Malmendal, A., Evenäs, J., Forsen, S. and Akke, M. (1999) *J. Mol. Biol.*, **293**, 883–899.
- Mandel, A.M., Akke, M. and Palmer, A.G., III (1995) *J. Mol. Biol.*, **246**, 144–163.
- Marion, D., Ikura, M., Tschudin, R. and Bax, A. (1989) *J. Magn. Reson.*, **85**, 393–399.
- Mauguen, Y., Hartley, R.W., Dobson, G., Bricogène, G., Chothia, C. and Jack, A. (1982) *Nature (London)*, **297**, 162–164.
- Matouschek, A., Serrano, L. and Fersht, A.R. (1992) *J. Mol. Biol.*, **224**, 819–835.
- Mime, S., Tale, S., Ueda, T., Kainosho, M. and Imoto, T. (1999) *J. Mol. Biol.*, **286**, 1547–1565.
- Okorokov, A.L., Hartley, R.W. and Panov, K.I. (1994) *Protein Express. Purif.*, **5**, 547–552.
- Palmer, A.G., III, Cavanagh, J., Wright, P.E. and Rance, M. (1991) *J. Magn. Reson.*, **93**, 151–170.
- Palmer, A.G., III, Williams, J. and McDermott, A. (1996) *J. Phys. Chem.*, **100**, 13293–13310.
- Peng, J.W. and Wagner, G. (1994) *Methods Enzymol.*, **239**, 563–596.
- Prompers, J.J., Groenewegen, A., Hilbers, C.W. and Pepermans, H.A.M. (1999) *Biochemistry*, **38**, 5315–5327.
- Sanz, J.M., Johnson, C.M. and Fersht, A.R. (1994) *Biochemistry*, **33**, 11189–11199.
- Schurr, J.M., Babcock, H.P. and Fujimoto, B.S. (1994) *J. Magn. Reson.*, **B105**, 211–224.
- Skelton, N.J., Palmer, A.G., Akke, M., Kördel, J., Rance, M. and Chazin, W.J. (1993) *J. Magn. Reson.*, **B102**, 253–264.
- Slijper, J., Boelens, R., Davis, A.L., Konings, R.N.H., Marel, G.A. van der, Boom, J.H. van and Kaptein, R. (1997) *Biochemistry*, **36**, 249–254.
- Stivers, J.T., Abeygunawardana, C. and Mildvan, A.S. (1996) *Biochemistry*, **35**, 16036–16047.
- Tjandra, N., Garrett, D.S., Gronenborn, A.M., Bax, A. and Clore, G.M. (1997) *Nature Struct. Biol.*, **4**, 443–449.
- Tjandra, N., Feller, S.E., Pastor, R.W. and Bax, A. (1995) *J. Am. Chem. Soc.*, **117**, 12562–12566.
- Vis, H., Vorgias, C.E., Wilson, K.S., Kaptein, R. and Boelens, R. (1998) *J. Biomol. NMR*, **11**, 265–277.
- Werten, S., Wechselberger, R., Boelens, R., Vliet, P.C. van der, and Kaptein, R. (1999) *J. Biol. Chem.*, **274**, 3693–3699.
- Yang, D. and Kay, L.E. (1996) *J. Mol. Biol.*, **263**, 369–382.
- Ye, J., Mayer, K.L. and Stone, M.J. (1999) *J. Biomol. NMR*, **15**, 115–124.
- Zhang, P., Dayie, K.T. and Wagner, G. (1997) *J. Mol. Biol.*, **272**, 443–455.
- Zheng, Z., Czaplicki, J. and Jardetzky, O. (1995) *Biochemistry*, **34**, 5212–5223.